DOI: 10.1021/ma100126n

Macromolecules
ARTICLE

Excited-State Intramolecular Proton Transfer in Imide Compounds and its Application to Control the Emission Colors of Highly Fluorescent Polyimides

Junji Wakita,[†] Shinsuke Inoue,[‡] Noriyuki Kawanishi,[‡] and Shinji Ando*,[†]

[†]*Department of Chemistry and Materials Science, Tokyo Institute of Technology, Ookayama, Meguro-ku, Tokyo 152-8552, Japan, and* [‡]*Research Laboratory, MANAC Incorporated, Fukuyama, Hiroshima, 721-0956, Japan*

Received January 18, 2010; Revised Manuscript Received March 3, 2010

ABSTRACT: A new molecular design concept for colorless and multicolor light-emitting polyimides (PIs) based on excited-state proton transfer is proposed. The ultraviolet−visible optical absorption spectra and fluorescence spectra of PIs containing hydroxy groups in their anhydride moieties and their corresponding imide compounds were extensively investigated. *N*-Cyclohexyl-3-hydroxyphthalimide (3HNHPI), which forms intramolecular hydrogen bonding between the hydroxy group and imide carbonyl group, exhibited an excited-state intramolecular proton transfer (ESIPT) emission at 534 nm with excitation at 332 nm having a large Stokes' shift of 11394 cm^{-1}. The highly fluorescent PIs, prepared from 4,4′-oxidiphthalic dianhydride (ODPA) and 4,4′-diaminocyclohexylmethane (DCHM) end-capped with 3-hydroxyphthalic anhydride, are colorless and exhibited two characteristic fluorescence peaks at 400 and 530 nm with excitation at 340 nm. These PIs showed gradated multicolor emission (blue, light-blue, white, and light-green) depending on the amount of fluorescent termini while maintaining colorless and transparence. It was clarified that ESIPT emission is a useful tool for controlling the absorption and fluorescence properties of PIs.

1. Introduction

Fully aromatic polyimides (Ar-PIs) are well-known high-performance engineering plastics exhibiting outstanding physical and chemical properties: thermal and chemical stability, flame resistance, radiation resistance, mechanical strength, and flexibility.[1] Ar-PIs synthesized from pyromellitic dianhydride and bis(4-aminophenyl) ether (PMDA/ODA) and from 3,3′,4,4′-biphenyltetracarboxylic dianhydride and *p*-phenylenediamine (*s*-BPDA/PDA) are representative ones, and they have been commercialized as Kapton-H and Upilex-S, respectively. Ar-PIs have been used in a wide range of high-tech fields, such as aerospace, electric, electronic and photonic applications. Additionally, fluorinated PIs and/or semialiphatic PIs (Al-PIs) have attracted much interest as a new class of electronic and optical material due to their colorlessness, high transparency, low refractive indices, and low birefringence.[2−9] For example, they have been applied to waveguides and optical peripheral components with highly controlled optical properties in the visible and near-IR regions.[5]

The origin of the absorption bands of PIs can be classified into two types of electronic transitions.[4,10] The first one is a "locally excited" (LE) transition which occurs in the dianhydride moiety, and the second one is a "charge transfer" (CT) transition originating from the CT complexes formed between the electron-donating diamine and the electron-accepting dianhydride moieties. Although the former absorption bands are observed in all kinds of PIs, i.e., fully aliphatic PIs, Al-PIs and Ar-PIs, the latter absorption bands are generally observed only in Ar-PIs because of the high electron-donating and electron-accepting properties of aromatic diamine and dianhydride, respectively.[3,4,6,7,11] The energy gaps of CT transitions, which are smaller than those of LE transitions, displace the absorption edges of Ar-PI films to the longer wavelength region ($\lambda > 400$ nm, visible region), which is the essential cause for the orange to brown colors of conventional Ar-PI films. In the case of PMDA/ODA, the CT absorption and emission bands are observed at around 400 and 600 nm, respectively.[12,13] In addition, Hasegawa and co-workers[4,10] reported that *s*-BPDA/PDA exhibited a broad CT emission band at 560 nm, and the excitation spectrum coincided with its absorption spectrum. They concluded that the CT emission of the PI is caused not only by direct excitation at the CT absorption band, but also by LE transition within the *s*-BPDA moiety, followed by energy transfer from the LE to the CT state. The photoluminescence quantum efficiency (Φ) of CT emission is generally very low; for example, the Φ value of PMDA/ODA was reported to be 9.7×10^{-7}.[13]

Very recently, the present authors[14] proposed the following molecular design concept for synthesizing 'highly fluorescent PIs' without fluorescent-dyes:

(1) Use of alicyclic diamines: The Φ values of the CT emissions in PIs are very low due to the very small oscillator strengths of CT transitions. The use of alicyclic diamines effectively prevents CT complex formation owing to their low electron-donating properties, and hence the Al-PIs can exhibit LE fluorescence.

(2) Use of aromatic dianhydrides with extended conjugation: The Φ values of LE(n−π^*) emissions are also very low, which is due to the very small oscillator strengths of LE(n−π^*) transitions. Since the energy of the LE(π−π^*) state rapidly falls by increasing the conjugation length, the Al-PIs prepared from dianhydrides having extended conjugation with biphenyl or ether linkages exhibit efficient LE(π−π^*) emissions whose Φ is significantly higher than that of LE(n−π^*) emissions.

*Corresponding author. E-mail: sando@polymer.titech.ac.jp. Telephone: +81-3-5734-2137. Fax: +81-3-5734-2889.

 Published on Web 03/16/2010

Scheme 1. Schematic Representation of Excited-State Proton Transfer (ESIPT) Photocycle Scheme

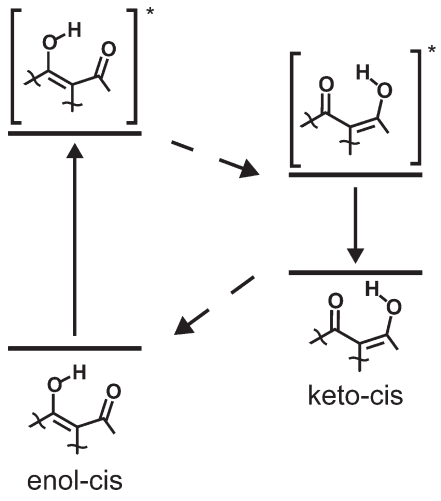

(3) Use of dianhydrides with flexible internal linkages: The dense chain packing of PIs lowers the Φ values due to strong interchain interactions. Dianhydrides involving flexible linkages such as ether groups in the main chain lead to loose chain packing of PIs, which increases the Φ values.

Although the highly fluorescent PIs thus obtained, e.g. ODPA/DCHM (poly(4,4′-dicyclohexylmethylene 3,3′,4,4′-oxidiphthalic imide), exhibit high transparency in the visible region, they demonstrate only blue emission with excitation by UV light. Our group has also reported that Al-PIs synthesized from perfluorinated aromatic dianhydrides, such as 1,4-bis(3,4-dicarboxytrifluorophenoxy)tetrafluorobenzene dianhydride and difluoropyromellitic dianhydride, exhibited strong bluish green and red emissions, respectively.[15] This indicates that fluorinated aromatic dianhydrides can provide fluorescent PIs with red-shifted emissions. However, fluorinated PIs exhibited strong absorption at the shorter wavelengths in the visible region (400−600 nm), which deteriorates optical transparency. Since colorless and highly transparent PI films are preferable for optical and photonic applications, a new molecular design concept for controlling the fluorescent colors (emission wavelengths) while maintaining high optical transparency has been strongly required.

It has been reported that certain types of aromatic compounds having acidic and basic groups undergo excited-state intramolecular proton transfer (ESIPT) as a result of increases in acidity and basicity upon excitation. 3-Hydroxyflavone derivatives,[16−19] 2-(2′-hydroxyphenyl)benzazole[20−29] (benzoxazole (HBO),[23−25] benzimidazole (HBI),[26−29] and benzothiazole (HBT)[20−22]), 1-hydroxy-2-acetonaphthone,[30−32] salicylideneaniline,[33−35] 2-(2′hydroxyphenyll)perimidine,[36] and 2,5-diphenyl-1,3,4-oxadiazole[37,38] are representative ESIPT compounds, in which an acidic and a basic groups are in close proximity with the appropriate geometry for strong intramolecular hydrogen bonding (*intra*-HB). These compounds have been applied to laser dyes,[39] high-energy radiation detectors,[40] UV-photostabilizers,[41] fluorescent probes,[42] and all-optical wavelength converter using a polymeric Mach−Zehnder interferometer.[43] A typical photophysical process observed in such ESIPT compounds is depicted in Scheme 1. Excitation of an enol−cis isomer with UV radiation forms the Franck−Condon S_1 excited state, which rapidly undergoes ESIPT to produce an excited keto−cis tautomer. In the successive decay to the ground state by radiative or nonradiative processes, a reverse proton transfer occurs to yield the original ground-state enol−cis isomer. The keto−cis tautomer exhibits an emission at a longer wavelength than that of the enol−cis isomer, resulting in a large Stokes' shift. Recently, ESIPT compounds have attracted much interest as emitting materials. Park et al. reported a white-light-emitting molecule utilizing ESIPT phenomenon which is composed of covalently linked blue- and orange-light-emitting moieties between which energy transfer is entirely attenuated.[44] In addition, polymeric materials having ESIPT units in the main chain or side chain have also been reported.[25,45−50] Chu et al. reported that a π-conjugated polymer with HBO units in the main chain exhibited ESIPT emission at 619 nm with excitation at 425 nm.[25] Accordingly, if Al-PIs are designed to incorporate ESIPT units in the main chain, they could be candidates for another type of "highly fluorescent PI" in which the absorption and fluorescence wavelengths can be well controlled. On the basis of the above literature, ESIPT emission should be observed also in imide compounds which form *intra*-HB between imide carbonyls and a phenolic hydroxy group. However, to the best of our knowledge, no such ESIPT behavior has been reported for imide compounds.

In this paper, first, the ultraviolet−visible (UV/vis) optical absorption and fluorescence spectra of low-molecular-weight imide compounds having a hydroxy group in the anhydride moiety are examined. To clarify the effect of the hydroxy group on the absorption and fluorescence properties of imide compounds, the density functional theory (DFT) calculations are utilized. Second, the absorption and fluorescence spectra of a series of Al-PIs (ODPA/DCHM) which are end-capped with anhydrides having a hydroxy group are investigated to establish a novel molecular design concept for highly fluorescent PIs exhibiting high transparency in the visible region and gradated multicolor fluorescent emission with excitation by UV light.

2. Experimental Section

2.1. Materials. Phthalic anhydride (PA), purchased from Kanto Chemical Co., Inc., was purified by sublimation under reduced pressure. 3-Hydroxyphthalic anhydride (3HPA), purchased from Aldrich, was used as received. 4-Hydroxyphthalic anhydride (4HPA), supplied by MANAC INC, was used as received. 4,4′-Oxydiphthalic dianhydride (ODPA), supplied by Shanghai Institute of Synthetic Resins, was dried at 150 °C for 12 h under reduced pressure. 4,4′-Diaminocyclohexylmethane (DCHM), purchased from Tokyo Kasei Kogyo Co., Ltd., was recrystallized from *n*-hexane and sublimed under reduced pressure. *N,O*-Bis(trimethylsilyl)trifluoroacetamide (99$^+$%, BSTFA) and *N,N*-dimethylacetamide (anhydrous, DMAc), purchased from Aldrich, were used as received.

2.2. Synthesis of Imide Compounds and Preparation of Polyimide Films. The molecular structures of low-molecular-weight imide compounds (*N*-cyclohexylphthalimide (NHPI), *N*-cyclohexyl-3-hydroxyphthalimide (3HNHPI), and *N*-cyclohexyl-4-hydroxyphthalimide (4HNHPI) are shown in Chart 1. All imide compounds were prepared by thermal imidization of the corresponding precursors (amic acid) in the presence of a phosphorus oxide catalyst at 140−155 °C, and they were recrystallized from suitable solvents.

The precursors of ODPA/DCHM PIs, poly(amic acid) silylester (PASE), were prepared by the *in situ* silylation method reported by Matsumoto[51] and Oishi.[52,53] The molecular structures of ODPA/DCHM with end groups are also shown in Chart 1. Hereafter, ODPA/DCHM without end groups will be abbreviated as PI-ne, and ODPA/DCHM end-capped by PA, 4HPA, and 3HPA will be abbreviated as PI-PA, PI-4HPA and PI-3HPA, respectively. In the case of PI-ne, DCHM was dissolved in DMAc, stirred for a few minutes, and then a 1.05 M amount of BSTFA was slowly added. An equimolar amount of ODPA was then added and stirred at room temperature for 48 h to give a PASE solution. The trimethylsilylation of the amino groups of diamines by BSTFA can avoid salt formation between

Chart 1. Structures of Imide Compounds and End-Capped Polyimides

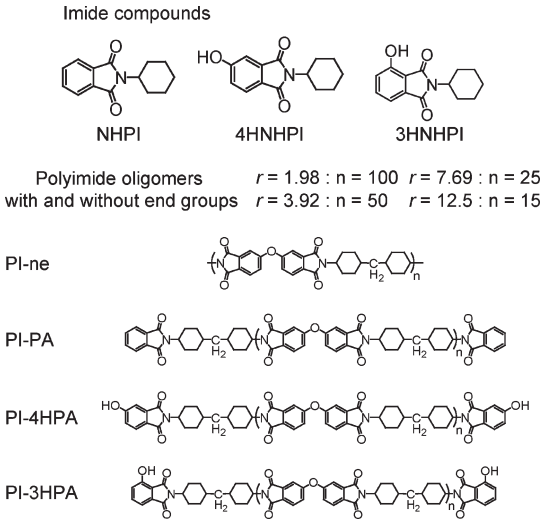

unreacted amino and carboxyl groups. In the case of ODPA/DCHM with end groups, the molar ratio of the end group (r) is defined as follows:

$$r = \frac{100 \times m(\text{end})}{m(\text{end}) + 2m(\text{ODPA})} \quad (1)$$

where m(end) and m(ODPA) are the molar quantities of the end group and dianhydride, respectively. On the basis of the definition, the number-average degree of polymerization (n) of PASE is given by $(-1 + 200/r)$, in which the varied values of r are 1.98, 3.92, 7.69 and 12.5, which corresponds to n = 100, 50, 25 and 15, respectively. The trimethylsilylated DCHM solution was prepared by the same procedure as that for PI-ne. A $(100 - r)/100$ molar amount of ODPA was then added to the solution and stirred at room temperature for 24 h. A $r/50$ molar amount of the anhydride (PA, 3HPA, 4HPA) was added and stirred at room temperature for 24 h to give a PASE solution. The anhydride molecules react with the terminal amino groups of the PASE chains, which gives terminal-modified PASE chains. PI films were subsequently prepared by thermal imidization of the corresponding precursors. A viscous PASE solution was spin-coated onto a fused silica (amorphous SiO_2) substrate, followed by soft-baking at 70 °C for 1 h and subsequent thermal imidization by a one-step imidization procedure: the final curing conditions were 220 °C for 1.5 h. The heating rate was 4.6 °C/min from 70 to 220 °C. All curing procedures were conducted under nitrogen flow.

2.3. Measurements. Solutions of imide compounds were prepared with concentrations of from 10^{-4} to 10^{-6} M. Chloroform ($CHCl_3$ 99.9%, Kanto Chemical Co., Inc., fluorescence grade) and trifluoroacetic acid (99.9%, Fluka, spectroscopic grade) were used without further purification. The UV/vis absorption spectra of solution and film samples were measured with a Hitachi U-3500 spectrophotometer. The fluorescence spectra of solution and film samples were measured by a Hitachi F-4500 fluorescence spectrometer equipped with a photomultiplier tube, HAMAMATSU R3896 and R928, respectively. The fluorescence spectra of the solutions were measured without degassing. The front-face method was adopted for the film samples to reduce self-absorption of emitted fluorescence. The emission spectra were measured with excitation at the peak wavelengths (λ_{ex}) of corresponding excitation spectra. In contrast, the excitation spectra were measured by monitoring the fluorescence intensities at the peak wavelengths (λ_{em}) of emission spectra. The measured spectra were not corrected for the sensitivity of photomultiplier tubes to fluorescence wavelengths. The photoluminescence quantum efficiencies of the solution and film samples were measured in another way by using a calibrated integrating sphere (HAMAMATSU C9920) connected to a multichannel analyzer (HAMAMATSU C7473) via an optical fiber link. In this measurement, the samples were excited at a controlled λ_{ex} using a monochromated xenon light source, and the solution samples were degassed by argon prior to measurements. The fluorescence lifetimes of the film samples were acquired with a HAMAMATSU fluorescence lifetime instrument. The system uses a pulsed nitrogen-gas laser (λ = 337 nm, pulse width = 500 ps) as an excitation source combined with a streak camera (C4334) and a spectro-photometer (C5908). The lifetime data were analyzed using a multiexponential decay analysis program. The Fourier transformed infrared (FT-IR) absorption spectra of KBr pellets containing imide compounds were measured in the range 400−4000 cm^{-1} using a Thermo-Nicolet Avatar-320 spectrometer. FT-IR absorption spectra of PI films were measured in the range of 650 to 4000 cm^{-1} using a Thermo-Fisher Avatar-320 spectrometer equipped with a Thunderdome attenuated total reflection (ATR) attachment (incident angle 45°). The prism (internal reflection element) was made of germanium crystal with a refractive index of 4.0. All optical measurements were conducted at ambient temperature without humidity control. Solution-state ^{13}C NMR spectra were measured with a JEOL AL-400 spectrometer operating at a ^1H resonance frequency of 400 MHz. The chemical shifts were reported in ppm (δ) using tetramethylsilane (TMS) as the standard. Thermogravimetric analyses (TGA) were conducted with a Shimadzu DTG-60 analyzer with a heating rate of 10 °C/min. The film thicknesses of the PIs were measured with a probe-pin-type surface profilometer (DEKTAK-III).

2.4. Quantum Chemical Calculation. The density functional theory (DFT), with the three-parameter Becke-style hybrid functional (B3LYP),[54−56] was adopted for obtaining the electronic structures and spectroscopic properties of the imide compounds. DFT and time-dependent DFT (TD-DFT) geometry optimizations with the 6-311G(d) basis set were performed for the ground (S_0) and first singlet excited (S_1) states, respectively. The 6-311G(d) basis set was also utilized for the calculation of IR spectra at the S_0 geometry. For reproducing the shapes of the experimental IR spectra, each calculated transition was replaced by a Gaussian broadening function with a half-width at half-maximum (HWHM) of 4 cm^{-1}. The calculated wavenumbers were scaled down by multiplying by a single factor of 0.98 for correcting vibrational anharmonicity, basis set truncation, and the neglected part of electron correlation. The basis set of 6-311+G(2d,p) was utilized for calculations of magnetic shielding at the S_0 geometry. The basis set of 6-311++G(d,p) was used for generating molecular orbitals and calculating vertical excitation wavelengths and oscillator strengths (f) at the S_0 and S_1 geometries. The former excitation corresponds to optical absorption. According to Kasha's rule, the $S_0 \rightarrow S_1$ transition at the S_1 geometry corresponds to emission. All calculations were performed with the Guassian-09 A.02 program package[57] which implements analytical gradients at the TD-DFT level. This package is installed in the Global Scientific Information and Computing Center (GSIC), Tokyo Institute of Technology.

3. Results and Discussion

3.1. Imide Compounds. *IR Spectra of Imide Compounds.* Figure 1 shows the FT-IR spectra of three imide compounds. All compounds demonstrated peaks at 1360, 1710, and 1780 cm^{-1}, which are assignable to the in-plane stretching of imide C−N bonds, and the asymmetric and symmetric stretching of C=O bonds in the imide rings, respectively. Additionally, no peaks assignable to the C−N stretching and N−H bending of amide groups (1530 cm^{-1}) or the stretching of carboxylic acid and/or amide C=O bonds (1690 cm^{-1}) were observed. These results indicated the completion of thermal imidization of the precursor compounds. Note that

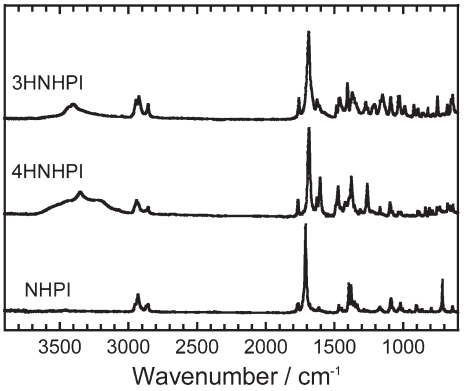

Figure 1. IR spectra of imide compounds NHPI, 4HNHPI, and 3HNHPI.

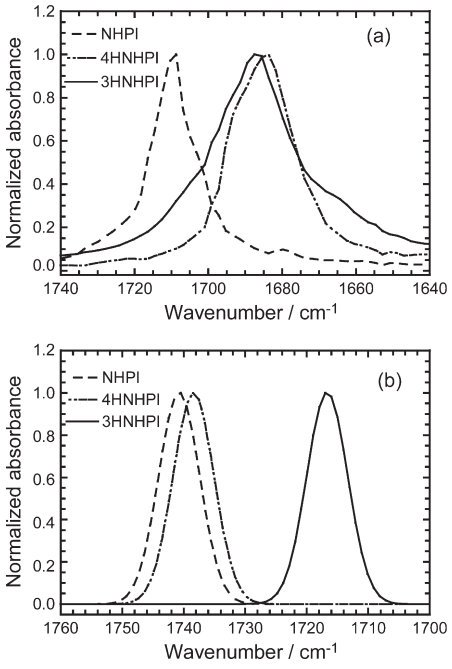

Figure 2. (a) Experimental and (b) calculated IR spectra of NHPI, 4HNHPI and 3HNHPI. The spectra have been normalized at the asymmetric C=O stretching bands. The calculated IR spectra were obtained at the DFT B3LYP/6-311G(d) level, and scaling factor was 0.98.

broad O−H stretching bands are clearly observed at around 3500 cm^{-1} in 4HNHPI and 3HNHPI, which indicates that phenolic hydroxy groups were not deteriorated during imidization.

Parts a and b of Figure 2 show the experimental and calculated IR spectra normalized by the asymmetric carbonyl stretching (ν_{CO}) peaks of three imide compounds, respectively. The peak of NHPI (exp, 1709 cm^{-1}; calcd, 1741 cm^{-1}) is ascribed to the ν_{CO} without *intra*-HB and intermolecular hydrogen bonding (*inter*-HB) because NHPI possesses no hydrogen-donating groups. In the case of 4HNHPI, which cannot form *intra*-HB, the experimental ν_{CO} peak (1680 cm^{-1}) is shifted to the lower wavenumber by 29 cm^{-1} relative to that of NHPI. This should be caused by *inter*-HB between the imide carbonyl and a phenolic hydroxy group of another molecule. It has been reported that the formation of hydrogen bonding causes a lower wavenumber shift of ν_{CO} peaks.[58] The formation of *inter*-HB is also supported by the fact that 4-aminophthalimide, which has a hydrogen-donating group at the same position as 4HNHPI, forms *inter*-HB between the imide carbonyl and an amino group of another molecule.[59] In fact, the calculated ν_{CO} peak of 4HNHPI (1738 cm^{-1}) appears at the same position as NHPI (1741 cm^{-1}) because the DFT calculation does not include *inter*-HB effects. The observed peak shift induced by *inter*-HB was reproduced by the DFT calculation of a hydrogen-bonded dimer of 4HNHPI, in which a peak shift of 31 cm^{-1} was obtained (see Figure S1 in Supporting Information). The absence of peaks at around 1700 cm^{-1} clearly indicates that most of the 4HNHPI molecules form *inter*-HB.

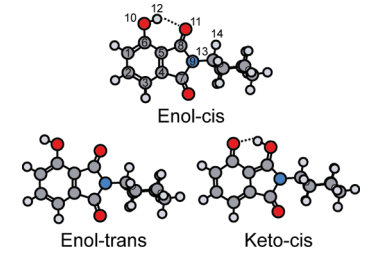

Figure 3. Enol−cis isomer, enol−trans isomer, and keto−cis tautomer structures of 3HNHPI. Dotted lines represent intramolecular hydrogen bondings.

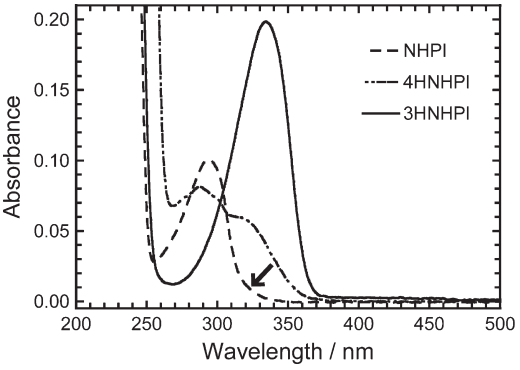

Figure 4. Optical absorption spectra of NHPI, 4HNHPI, and 3HNHPI (5×10^{-5} M) in a $CHCl_3$ solution. The arrow denotes a weak absorption tailing of a NHPI solution.

As shown in Figure 3, 3HNHPI is expected to have enol−cis and enol−trans isomers plus keto−cis tautomer. According to the DFT calculations, the total energies of the enol−trans isomer and keto−cis tautomer are higher than that of the enol−cis isomer by 29 and 85 kJ/mol, respectively. Assuming the Boltzman distribution at room temperature, the ratios of [enol−trans]/[enol−cis] and [keto−cis]/[enol−cis] are estimated to be 7.0×10^{-6} and 1.3×10^{-15}, respectively, which suggests that the enol−trans isomer and the keto−cis tautomer are negligible in the ground state. Hence, the calculated IR spectrum of the 3HNHPI enol−cis isomer is shown in Figure 2b. In the case of 3HNHPI, both the experimental and calculated ν_{CO} peaks were shifted to a lower wavenumber relative to those of NHPI (exp, 1680 cm^{-1}; calcd, 1717 cm^{-1}), which should be mainly caused by the formation of *intra*-HB between the imide carbonyl and a phenolic hydroxy group. The H12−O11 (as labeled in Figure 3) distance (2.15 Å) at the optimized geometry in the S_0 state of 3HNHPI is a typical value between hydrogen and oxygen atoms which form *intra*-HB.[60]

UV/Vis and Fluorescence Spectra of Imide Compounds. Figures 4 and 5 respectively show the UV/vis and fluorescence spectra ((a) excitation and (b) emission spectra) of NHPI, 4HNHPI, and 3HNHPI in a $CHCl_3$ solution (5×10^{-5} M). Table 1 summarizes the absorption peak wave-

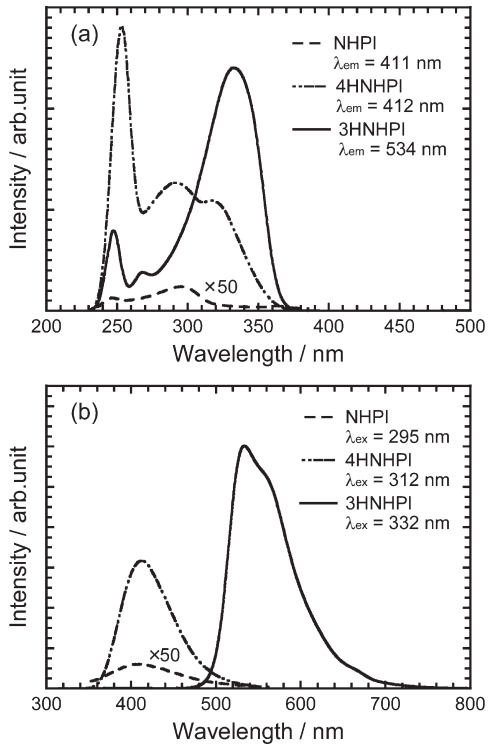

Figure 5. Fluorescence spectra of NHPI, 4HNHPI and 3HNHPI (5×10^{-5} M) in a $CHCl_3$ solution: (a) excitation spectra monitored at λ_{em}, (b) emission spectra excited at λ_{ex}.

lengths (λ_{abs}), molar absorption coefficients (ε), excitation and emission wavelengths (λ_{ex}, λ_{em}), Stokes' shifts (ν), and photoluminescence quantum efficiencies (PLQE, Φ) for the three compounds. Stokes' shift is defined as the wavenumber difference between the transition energies for excitation and emission peaks. Table 2 lists the vertical excitation wavelengths, oscillator strengths (f), contributing molecular orbitals (MO), assignments of electron transitions, and the contribution of each transition calculated for the imide compounds at the S_0 geometry. Here, HOMO$-m$ and LUMO$+m$ denote the $(m+1)$th highest occupied MOs and $(m+1)$th lowest unoccupied MOs, respectively. According to the time-dependent (TD) perturbation theory, the wave function of the system, Ψ, is expressed as $\Psi = \sum_k c_k \exp(-iE_k t/\hbar)\, \Phi_k$, where c_k denotes the expansion coefficient, and Φ_k the eigen functions of the time-independent Schrödinger equation having eigen values of E_k. Values of c_k larger than 0.1 were obtained by TD-DFT calculations, and the contribution of each Φ_k to the electronic transitions can be approximated by the normalized expansion coefficient which is defined as ${c_i}^2/\sum_i {c_k}^2$. Table 3 lists the calculated emission wavelength ($\lambda_{em,calcd}$) and assignments for the imide compounds computed at the S_1 geometry.

NHPI exhibits an absorption peak at 290 nm and a weak absorption tailing at around 320 nm, as indicated by the arrow in Figure 4. The spatial distributions of the MOs are illustrated in Figure 6. The HOMO-1, which is localized around the lone pairs of carbonyl oxygens and the imide nitrogen, is regarded as a lone pair (n) orbital. On the other hand, HOMO-3, HOMO-2, HOMO, LUMO and LUMO$+1$ are delocalized over the anhydride moiety, and hence they are regarded as π orbitals. Accordingly, the calculated transition at 323.7 nm ($S_0 \rightarrow S_1$) is characterized as an LE(n$-\pi^*$) transition, and those at 305.1 nm ($S_0 \rightarrow S_2$) and 271.6 nm ($S_0 \rightarrow S_4$) are characterized as LE($\pi-\pi^*$) transitions (see Table 2). The wavelength of the $S_0 \rightarrow S_1$ transition with small f values (0.0001) is in accord with the tailing of absorption in the experimental UV/vis spectrum (around 320 nm), which indicates that the weak tailing is attributable to the LE(n$-\pi^*$) band. In contrast, the wavelength of the $S_0 \rightarrow S_4$ transition with a large f value (0.0342) is close to that of the absorption peak (290 nm), which indicates that the absorption band is attributable to the LE($\pi-\pi^*$) band. NHPI shows excitation and emission peaks at 295 and 411 nm, respectively (Figure 5). Hereafter, the fluorescence peak positions will be expressed as ($\lambda_{ex}/\lambda_{em}$)=(295 nm/411 nm). The transition for excitation is assignable to the LE($\pi-\pi^*$) transition because the λ_{ex} agrees with that of the LE($\pi-\pi^*$) absorption band (290 nm). In general, fluorescence is emitted by energy relaxation from the lowest excited state (S_1) to the ground state (S_0) after fast internal conversion from the S_i to S_1 states (Kasha's rule). Since the S_1 state of NHPI is an LE(n$-\pi^*$) state (see Table 2), fast internal conversion should occur from the higher LE($\pi-\pi^*$) state to the lowest LE(n$-\pi^*$) state when NHPI is excited at 295 nm. Hence, the emission peak at 411 nm is attributable to an LE(n$-\pi^*$) fluorescence. This assignment is verified by the fact that the λ_{em} agrees well with the calculated LE(n$-\pi^*$) emission wavelength (403.9 nm) (see Table 3). The experimental Φ value obtained by excitation at $\lambda_{ex} = 295$ nm was estimated as 0.007 by using an integrating sphere. PLQE can be theoretically expressed as follows:[61]

$$\Phi \propto \frac{k_e^0}{k_e^0 + \sum k_i} \tag{2}$$

$$k_e^0 = 3 \times 10^{-9} \bar{\nu}_0{}^2 \int \varepsilon \, d\bar{\nu} \cong \bar{\nu}_0{}^2 f \tag{3}$$

where $k_e{}^0$ is the radiative rate constant, $\sum k_i$ the sum of all nonradiative rate constants, $\bar{\nu}_0$ the energy corresponding to the maximum wavelength of absorption, ε the molar absorption coefficient, and f the oscillator strength for absorption. As shown in Table 2, the calculated oscillator strength of the LE(n$-\pi^*$) transition ($S_0 \rightarrow S_1$) is very small (0.0001), which results in a small $k_e{}^0$ of the LE(n$-\pi^*$) band (see eq 3). In addition, it was reported that the fast intersystem crossing from the $^1(n,\pi^*)$ to the $^3(\pi,\pi^*)$ state occurs in *N*-alkyl-substituted phthalimide[4,62,63] and subsequently radiationless $T_1 \rightarrow S_0$ intersystem crossing occurs at room temperature, which increases the $\sum k_i$. According to eq 2, the combination of small $k_e{}^0$ and large $\sum k_i$ values results in the low Φ value. Consequently, the very small Φ value experimentally obtained for the LE(n$-\pi^*$) fluorescence in NHPI should originate from the small oscillator strength of the LE(n$-\pi^*$) transition and the fast intersystem crossing.

4HNHPI shows two absorption peaks at 290 and 320 nm (Figure 4). The calculated transitions of 4HNHPI appearing at 326.2 nm ($S_0 \rightarrow S_1$) and 276.3 nm ($S_0 \rightarrow S_4$) with large f values (> 0.01) are assignable to LE($\pi-\pi^*$) transitions

Table 1. Experimental Absorption Wavelengths (λ_{abs}), Molar Absorption Coefficients (ε), Excitation and Emission Wavelengths (λ_{ex}, λ_{em}), Stokes' Shifts (ν) and Photoluminescence Quantum Efficiencies (Φ) of NHPI, 4HNHPI, and 3HNHPI (5×10^{-5} M) in a $CHCl_3$ Solution

imide compound	λ_{abs}/ nm	ε / $cm^{-1}\,M^{-1}$	λ_{ex}/ nm	λ_{em}/ nm	ν/ cm^{-1}[a]	Φ
NHPI	294	1947	295	411	9567	0.007
4HNHPI	320	1160	312	412	7720	0.255
3HNHPI	328	3661	332	534	11394	0.352

[a] $\nu = 10^7\,(1/\lambda_{ex} - 1/\lambda_{em})$.

Table 2. Calculated Electronic Transitions of NHPI, 4HNHPI, and 3HNHPI at the Optimized S_0 Geometry[a,b]

imide compound	state	transition wavelength/nm	oscillator strength	orbitals	character of transition	contribution
NHPI	S_1	323.7	0.0001	HOMO-1 → LUMO	n−π^*	1.00
	S_2	305.1	0.0005	HOMO → LUMO	π−π^*	1.00
	S_4	271.6	0.0342	HOMO-2 → LUMO	π−π^*	0.75
				HOMO → LUMO+1		0.17
				HOMO-3 → LUMO+1		0.08
4HNHPI	S_1	326.2	0.0128	HOMO-2 → LUMO	π−π^*	0.96
				HOMO → LUMO		0.04
	S_2	319.1	0.0001	HOMO-1 → LUMO	n−π^*	1.00
	S_4	276.3	0.0160	HOMO-2 → LUMO	π−π^*	0.45
				HOMO → LUMO+1		0.32
				HOMO-3 → LUMO		0.20
				HOMO-3 → LUMO+1		0.03
3HNHPI enol−cis	S_1	324.3	0.0930	HOMO-1 → LUMO+1	π−π^*	0.83
				HOMO → LUMO		0.13
				HOMO-1 → LUMO		0.04
	S_2	320.5	0.0001	HOMO-2 → LUMO	n−π^*	1.00
	S_3	304.0	0.0241	HOMO → LUMO	π−π^*	0.89
				HOMO-1 → LUMO		0.11
3HNHPI keto−cis	S_1	447.4	0.1438	HOMO → LUMO	π−π^*	0.92
				HOMO-2 → LUMO		0.05
				HOMO-2 → LUMO+1		0.03
	S_3	335.4	0.0175	HOMO-2 → LUMO	π−π^*	0.98
				HOMO → LUMO		0.02
	S_4	300.4	0.0001	HOMO-3 → LUMO	n−π^*	1.00

[a] TD-DFT calculations at the [B3LYP/6-311G++(d,p)] level. [b] Prohibited transitions ($f = 0$) are not listed.

Table 3. Calculated Emission Wavelengths ($\lambda_{em,calcd}$) and Their Assignments of NHPI, 4HNHPI, and 3HNHPI

imide compound	$\lambda_{em,calcd}$/nm	assignment
NHPI	403.9	n−π^*
4HNHPI	444.4	π−π^*
3HNHPI (enol−cis)	455.3	π−π^*
3HNHPI (keto−cis)	540.2	π−π^*

(see Table 2), and thereby these absorption bands are readily attributable to the LE(π−π^*) bands. A fluorescence peak is observed at (312 nm/412 nm) whose λ_{ex} value agrees with that of the LE(π−π^*) absorption band (Figure 5). Since the transition of excitation is attributable to the LE(π−π^*) transition of $S_0 \rightarrow S_1$, no internal conversion occurs after the excitation at 315 nm. Accordingly, the emission at 412 nm is assignable to an LE(π−π^*) fluorescence. The λ_{em} value is close to the calculated LE(π−π^*) emission wavelength (444.4 nm) (see Table 3), which also supports the assignment. The Φ value of 0.255 is much higher than that of NHPI (0.007), which should mainly originate from the large oscillator strength of the LE(π−π^*) transition (0.0128) and slow intersystem crossing from the $^1(\pi,\pi^*)$ to the $^3(\pi,\pi^*)$ state, according to eqs 2 and 3. Consequently, the introduction of a hydroxy group in the anhydride moiety lowers the (π,π^*) energy level, which significantly enhances the fluorescent efficiency of the LE emission.

3HNHPI shows an intense absorption peak at 332 nm (Figure 4). The calculated transition of the enol−cis isomer appearing at 324.3 nm ($S_0 \rightarrow S_1$) and 304.0 nm ($S_0 \rightarrow S_3$) with a large f value (>0.02) is attributable to the LE(π−π^*) transition (see Table 2), and hence the absorption band is readily assignable to an LE(π−π^*) band of the enol−cis isomer. The keto−cis tautomer of 3HNHPI shows a transition with a large f value (0.1438) at 447.4 nm (see Table 2). The absence of experimental absorption in the visible region (λ > 400 nm) indicates that few keto−cis tautomers exist in the ground state of 3HNHPI. A fluorescence peak observed at (328 nm/534 nm) exhibits a much larger Stokes' shift (12382 cm^{-1}) than that of 4HNHPI (7779 cm^{-1}) (see Table 1 and Figure 5). The transition for this excitation is

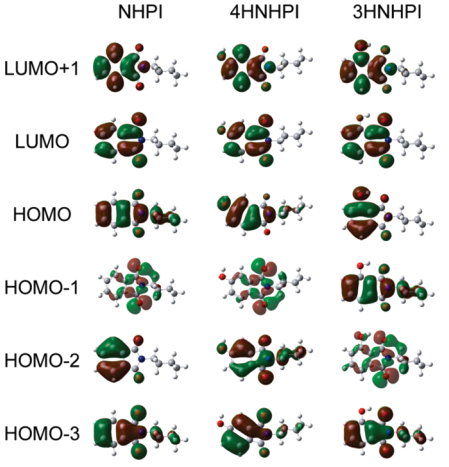

Figure 6. Calculated molecular orbitals of NHPI, 4HNHPI and 3HNHPI (TD-DFT method at the B3LYP/6-311++G(d,p) level). HOMO-m and LUMO+m denote the (m + 1)th highest occupied orbital and the (m + 1)th lowest unoccupied orbital, respectively.

attributable to the LE(π−π^*) transition of the enol−cis isomer because the λ_{ex} value agrees with that of the LE-(π−π^*) absorption band. In general, a large Stokes' shift suggests additional photophysical processes in the excited states, which frequently accompany substantial changes in the geometrical and electronic structures of molecules. One possible interpretation for the emission of 3HNHPI with a large Stokes' shift is that the enol−cis isomer underwent an excited-state intramolecular proton transfer (ESIPT) reaction after excitation at 328 nm, and subsequently a keto−cis tautomer was generated. This hypothesis is suggested by the following facts. First, the calculated emission wavelength of the keto−cis tautomer (540.2 nm) (see Table 3) is comparable to the experimental emission wavelength (534 nm). Second, the values of λ_{em} and the Stokes' shift are close to the typical values of ESIPT fluorescence in the literature.[16−19] For example, 3-hydroxyflavone exhibited an emission peak at 520 nm with excitation at 340 nm, in which the Stokes' shift is

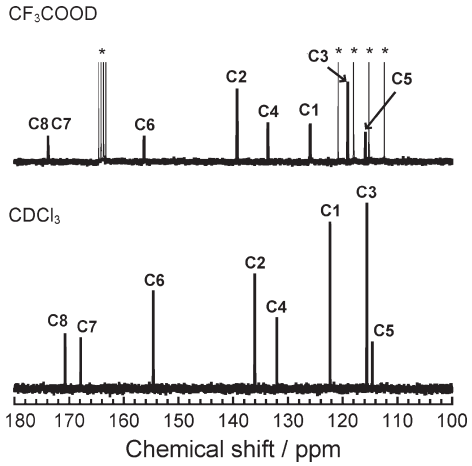

Figure 7. Solution-state ^{13}C NMR spectra of 3HNHPI in (a) $CDCl_3$ and (b) trifluoroacetic acid-*d* (TFA-*d*). Asterisks denote the signals from TFA. C1−C8 are as labeled in Figure 3.

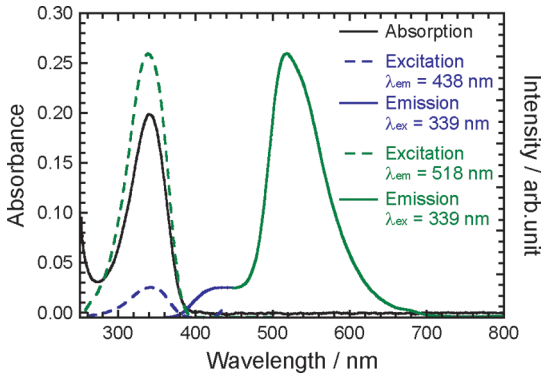

Figure 8. Optical absorption and fluorescence spectra of 3HNHPI (5×10^{-5} M) in a TFA solution.

10180 cm^{-1}.[19] Third, the ground-state equilibrium of 3HNHPI could be exclusively dominated by the enol−cis isomer which forms a stable six-membered circular structure with *intra*-HB (Figure 3). Similar structures are frequently found in typical ESIPT compounds.

The photophysical mechanism of 3HNHPI can be examined from the changes in the fluorescence spectrum of 3HNHPI in an acidic condition. Roberts and co-workers[27] have reported the solvent effects on the ESIPT fluorescence of 2-(2′-hydroxyphenyl)benzimidazole (HBI). By increasing the concentrations of trifluoroethanol (TFE) having a strong hydrogen-donating property, the emission originating from a keto−cis tautomer at 470 nm faded with the appearance of a weak emission between 350 and 400 nm. The newly appeared emission is attributable to that from the enol isomer, indicating a decrease in population of the ground-state molecules forming *intra*-HB. This indicates that the *intra*-HB was effectively weakened or disrupted by the formation of *inter*-HB between proton-accepting HBI and proton-donating TFE. If the emission of 3HNHPI at 530 nm originates from the keto−cis tautomer generated by the ESIPT reaction, the fluorescent emission from the enol isomer should be observed in an acidic condition.

To clarify the solvent effect on the hydrogen-bonded structure, ^{13}C NMR spectra of 3HNHPI were measured in a chloroform-*d* ($CDCl_3$) and trifluoroacetic acid-*d* (TFA-*d*) solution. The spectra in the range of from 100 to 180 ppm from TMS are shown in Figure 7. The signals were assigned based on the DEPT-135 measurement (selective observation of protonated carbons) with the aid of DFT magnetic shielding calculations (C1−C8, as labeled in the molecular structure in Figure 3). The DEPT-135 spectra and the magnetic shieldings (σ) are shown in Figures S2 and S3 in Supporting Information, respectively. The signals in the range of from 110 to 160 ppm are assignable to the aromatic carbons. The σ values of C8 and C7 for the enol−cis isomer are 5.41 and 8.42, respectively. The smaller σ of C8, which corresponds to the signal which resonated at a higher frequency, should originate from the *intra*-HB formed between imide carbonyl (C8) and the phenolic hydroxy group. Thereby, the signals at 170.7 and 167.9 ppm are assignable to C8 and C7, respectively. In the TFA-*d* solution, although the relative signal positions of the aromatic carbons are almost the same as in $CDCl_3$, only one signal was observed at 172.0 ppm for the carbonyl carbons. The *inter*-HB should be preferentially formed between imide carbonyl (C8) and TFA compared with the *intra*-HB because the acidity of TFA is much higher than that of the hydroxy group in 3HNHPI. Moreover, the *inter*-HB can also be formed between imide carbonyl (C7) and TFA, and thus the local electronic environments of C7 and C8 could be almost identical. This results in the one carbonyl carbon resonance of 3HNHPI in TFA-*d*.

Figure 8 shows the UV/vis and excitation/emission spectra of 3HNHPI in a TFA solution(5×10^{-5} M). The UV/vis spectrum demonstrated an absorption peak at 340 nm. According to the DFT calculation, the monocationic species of 3HNHPI should exhibit an electronic transition with a large *f* value (>0.1) at around 380 nm (see Chart S1 and Table S1 in Supporting Information). The absence of strong absorption above 380 nm in the experimental spectrum indicates that 3HNHPI was not protonated in TFA, and thus the absorption band is attributable to the LE($\pi-\pi^*$) band of the enol isomer which forms *inter*-HB. Unlike the $CHCl_3$ solution, two fluorescence peaks were observed at (339 nm/438 nm) and (339 nm/518 nm) in the TFA solution. The excitation transition is readily assignable to the LE-($\pi-\pi^*$) transition of the enol isomer because the value of λ_{ex} coincides with that of the LE($\pi-\pi^*$) absorption band. In the case of the former peak, the emission transition should be attributable to the LE($\pi-\pi^*$) fluorescence of the enol isomer which forms *inter*-HB, in which *intra*-HB was disrupted by TFA. This is because the value of λ_{em} is close to the calculated emission wavelength of the enol−cis isomer (455.3 nm) (see Table 3). Consequently, the latter fluorescence peak at (339 nm/518 nm), whose peak positions are close to those in the $CHCl_3$ solution, is readily attributable to the keto−cis tautomer of 3HNHPI formed via the ESIPT reaction. The ESIPT emission in TFA (λ_{em} = 518 nm) is slightly blue-shifted compared to that of the $CHCl_3$ solution (λ_{em} = 530 nm), which indicates that the keto−cis structure in the excited states was destabilized by the formation of *inter*-HB.

The schematic photophysical processes of 3HNHPI in the $CHCl_3$ and TFA solutions and their photo images under UV light (λ = 365 nm) irradiation are shown in Scheme 2, parts a and b, respectively. Both solutions exhibit green-color fluorescent emission. First, in the $CHCl_3$ solution, the excitation of the enol−cis isomer (E) with UV irradiation generates the excited enol−cis isomer (E*). Second, an adiabatic ESIPT reaction subsequently occurs, which yields the excited keto−cis tautomer (K*). Third, the excited keto−cis tautomer decays radiatively to the ground state of the keto−cis tautomer (K). Finally, a backward proton transfer promptly occurs, which restores the initial enol−cis isomer. According to eqs 2 and 3, the Φ value of 3HNHPI should be influenced by the oscillator strength (*f*) of the LE($\pi-\pi^*$) transition

Scheme 2. Schematic Representation of the Excitation and Emission Mechanism with the ESIPT Photocycle Scheme of Green-Light-Emitting 3HNHPI in a (a) $CHCl_3$ and (b) TFA Solution[a]

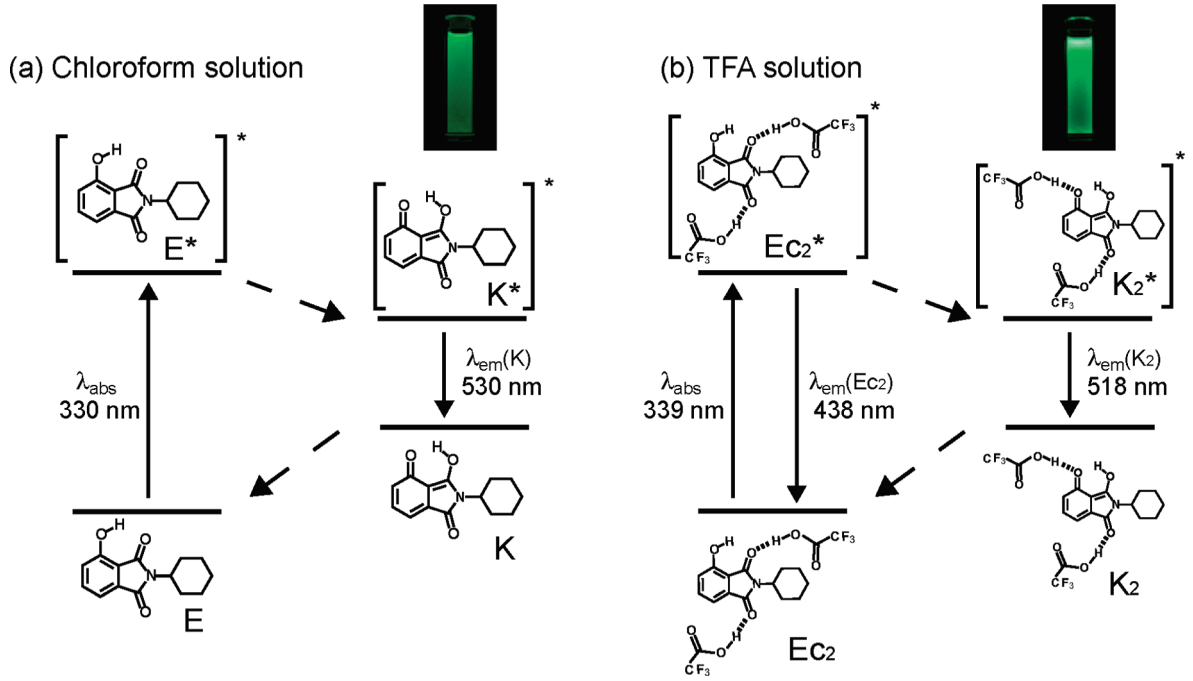

[a] Inset: photo images of 3HNHPI solutions under UV light (λ = 365 nm) irradiation.

($S_0 \rightarrow S_1$) of the keto−cis tautomer at the S_0 geometry. The calculated f value (0.1438) is much larger than that of the LE(π−π*) transition ($S_0 \rightarrow S_1$) of 4HNHPI (see Table 2), which should be the main cause of the higher Φ value of 3HNHPI in $CHCl_3$ (0.352) compared to that of 4HNHPI (0.255). In the case of the TFA solution, the enol−cis isomer with *inter*-HB (Ec_2*) should undergo the ESIPT reaction to produce the hydrogen-bonded keto−cis tautomer (K_2*). However, the ESIPT reaction is partially inhibited by *inter*-HB, and thus the LE(π−π*) emission attributable to Ec_2 was observed. The representative optimized geometrical parameters of the enol−cis isomer and the keto−cis tautomer in the S_0 and S_1 states are collected in Table S2 in Supporting Information (e.g., C1−H14, as labeled in the molecular structure in Figure 3). The figure in parentheses indicates the rate of change of geometric parameters upon one electron excitation. Large structural change does not occur upon excitation. In contrast, the distances of C6−O10 (1.289 Å) and O11−H12 (0.997 Å) of the keto−cis tautomer in the S_1 state are significantly shorter than those of the enol−cis isomer in the S_1 state (1.352 Å and 2.176 Å, respectively). In addition, the distances of O10−H12 (1.836 Å) and C8−O11 (1.317 Å) of the keto−cis tautomer are significantly longer than those of the enol−cis isomer (0.977 Å and 1.237 Å, respectively). However, the dihedral angles of C6−C5−C8-O11 and O10−H12−H11-O11 of both the enol−cis isomer and the keto−cis tautomer are equal to 0.0°. These results indicate that the H12 proton is transferred from O10 to O11 while maintaining a planar six-membered structure with *intra*-HB during the ESIPT process. It should be emphasized that, to the best of our knowledge, this is the first report on an aromatic imide compound which exhibits strong fluorescent emission via the ESIPT reaction.

3.2. Highly Fluorescent End-Capped PIs. *Characterization*. The ATR FT-IR spectra of the PI films are shown in Figure S4 in Supporting Information, and the completion of thermal imidization was confirmed by the C=O stretching and C−N stretching bands of the imide rings at 1780 and 1360 cm^{-1}, respectively. The film thicknesses and decomposition temperatures with 5% weight loss (T_d^5) are listed in Table 4. The TGA curves are shown in Figure S5 in Supporting Information. All PIs demonstrated good thermal stability without significant weight losses below 350 °C, which is due to the rigid molecular structure of the PIs. The relatively low T_d^5s observed for PI-4HPA (r = 7.69) and PI-3HPA (r = 12.5) could be due to the lower degree of polymerization.

Table 4. 5 wt % Decomposition Temperatures (T_d^5) and Film Thicknesses of PI Films

polyimide	r[a]	T_d^5/°C	thickness/μm
PI-PA	1.98	395	11.9
	3.92	389	9.7
	7.69	402	6.7
PI-4HPA	1.98	407	11.3
	3.92	400	7.3
	7.69	356	9.4
PI-3HPA	1.98	452	2.1
	3.92	441	15.1
	7.69	424	12.3
	12.5	372	3.0
PI-ne	−	414	4.4

[a] The r value represents the molar ratio of end group (see text).

UV/Vis and Fluorescence Spectra. The UV/vis spectra of the PI films are shown in Figure 9 ((a) PI-ne and PI-PA, (b) PI-4HPA, (c) PI-3HPA). The end-capped PIs exhibited absorption bands only in the UV region (< 400 nm), which is same as the spectrum of PI-ne. Note that, according to the DFT calculation, the keto−cis tautomer of 3HNHPI shows electronic transition at around 450 nm, as shown in section 3.1 (see Table 2). The absence of absorption bands in the visible region (> 400 nm) of PI-3HPA films indicates that 3HPA termini with enol structures should be dominant in the ground state. Figure 10 illustrates a photo image of PI-3HPA (r = 7.69) film under white light exposure (left-hand side). This film is highly transparent and completely colorless.

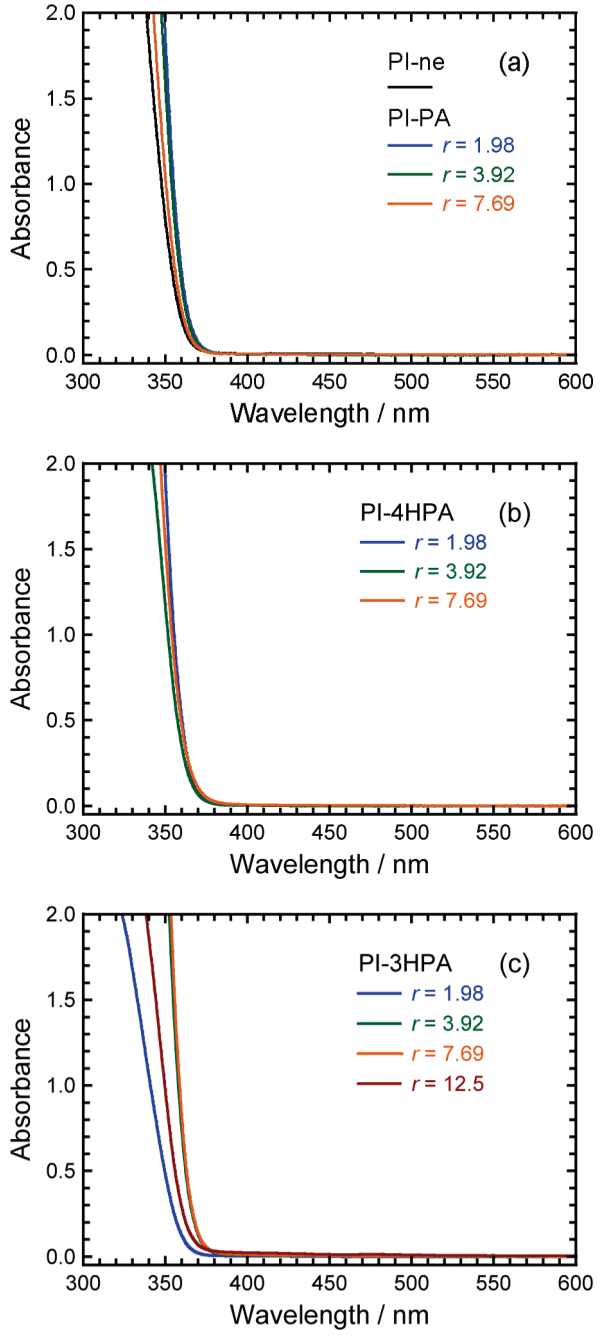

Figure 9. Optical absorption spectra of PI films, (a) PI-ne and PI-PA, (b) PI-4HPA, and (c) PI-3HPA.

Table 5 summarizes the excitation and emission wavelengths (λ_{ex}, λ_{em}), and PLQE (Φ) values observed for the PI films. Figure 11 demonstrates the normalized excitation (a) and emission (b) spectra of PI-ne, PI-PA, PI-4HPA, and PI-3HPA films (r = 7.69). The fluorescence intensities were normalized at λ_{ex} (around 340 nm) and λ_{em} (around 400 nm). In the case of PI-3HPA, the excitation spectrum monitored at 402 nm is normalized by the intensity at 320 nm. PI-ne, PI-PA, and PI-4HPA exhibited fluorescence excitation/emission peaks at (340 nm/400 nm), (344 nm/401 nm) and (345 nm/406 nm), respectively. These fluorescences are assignable to LE fluorescences emitted from imide rings in the main chain and/or end groups.[14] In the case of PI-3HPA, two fluorescence peaks were observed at (320 nm/402 nm) and (350 nm/535 nm). The former peak is assignable to an LE fluorescence of the main chain, similar

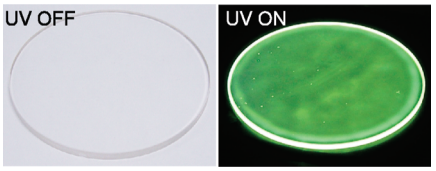

Figure 10. Photo images of a PI-3HPA (r = 7.69) film under white light (left) and UV (λ = 365 nm) irradiation (right).

Table 5. Excitation and Emission Wavelengths (λ_{ex}, λ_{em}), and Photoluminescence Quantum Efficiencies (Φ) of PI Films

polyimide	r	λ_{ex}/nm	λ_{em}/nm	Φ
PI-PA	1.98	348	402	0.076
	3.92	348	400	0.097
	7.69	344	401	0.113
PI-4HPA	1.98	350	402	0.070
	3.92	343	405	0.097
	7.69	345	406	0.058
PI-3HPA	1.98	339	400, 534	0.089
	3.92	352	402, 535	0.109
	7.69	350	402, 535	0.128
	12.5	341	401, 536	0.141
PI-ne	–	340	400	0.114

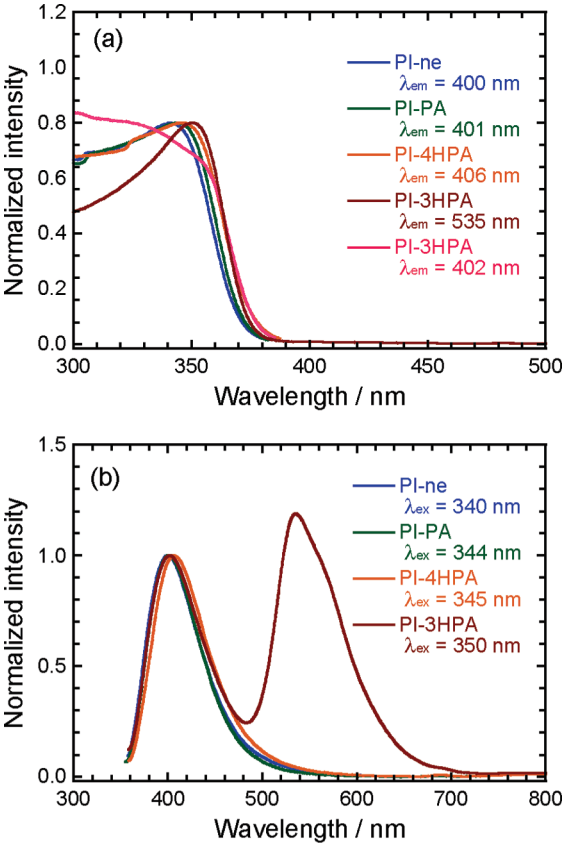

Figure 11. Fluorescence spectra of PI-ne, PI-PA, PI-4HPA, and PI-3HPA (r = 7.69) films: (a) excitation spectra monitored at λ_{em}; (b) emission spectra excited at λ_{ex}. The spectra have been normalized.

to PI-ne, PI-PA, and PI-4HPA. In contrast, the values of λ_{ex} and λ_{em} of the latter peak agree well with those of the ESIPT fluorescence observed for 3HNHPI in the $CHCl_3$ solution (see Figure 5 and Table 1), and hence the latter peak is attributable to the ESIPT fluorescence from 3HPA at the chain termini. As shown in Figure 10 (right), the colorless PI-3HPA film exhibits strong green-color fluorescent emission under UV light (365 nm) irradiation.

Figure 12 shows the emission spectra of PI-ne and PI-3HPA (r = 1.98−12.5). The intensities are normalized at around 400 nm. The relative intensity at 530 nm was significantly enhanced with an increase in r. To clarify the photophysical process of PI-3HPA, the fluorescence lifetimes (τ) were measured. Table 6 lists the τ values for the ESIPT emission (abbreviated as τ_{ESIPT}) and those of the LE emission (abbreviated as τ_{LE}) of PI-3HPA. Table 7 lists the τ_{LE} values of PI-PA and PI-4HPA as references. The values of τ_{LE} and τ_{ESIPT} were obtained from the fluorescence decay curves integrated in the wavelength range of 370−420 nm and 570−620 nm, respectively. The small dependence of τ_{LE} on r observed for PI-PA and PI-4HPA indicates that τ_{LE} is not influenced by the degree of polymerization. In contrast, the τ_{LE} value of PI-3HPA gradually decreased with an increase in r. This is a typical phenomenon for fluorescence via excited-state energy transfer, in which the fluorescence lifetime of the donor moiety decreases by increasing the acceptor moiety.[64] Hence, one can conclude that the intra- and/or interchain energy transfer from the imide ring in the main chain (donor) to the 3HPA (acceptor) moiety at the terminus occurs in the excited state. This significantly enhances the relative fluorescence intensity at 530 nm (Figure 12).

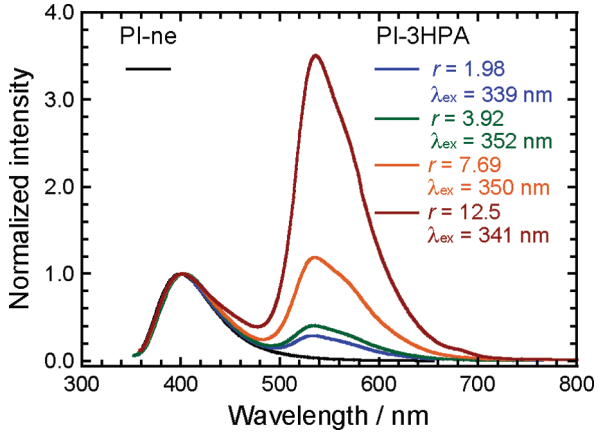

Figure 12. Influence of increasing amount of 3HPA termini on the emission spectra of PI-3HPA films excited at λ_{ex}. The spectra have been normalized.

Table 6. Fluorescence Lifetimes (τ) of the Emission Peaks Measured for PI-3HPA Films in the Shorter and Longer Wavelength Regions

r	τ_{LE}/ns[a] at 370−420 nm	τ_{ESIPT}/ns[b] at 570−620 nm
1.98	2.59	1.23
3.92	2.39	1.24
7.69	2.11	1.25
12.5	2.00	1.24

[a] τ for the LE emission of main chain. [b] τ for the ESIPT emission of end groups.

Table 7. Fluorescence lifetimes of PI-PA and 4HPA films

	τ_{LE}/ns	
r	PA	4HPA
1.98	2.73	2.69
3.92	2.74	2.68
7.69	2.71	2.62

All the photophysical processes of PI-3HPA are schematically illustrated in Figure 13. The first process is the conventional LE fluorescence consisting of the excitation (340 nm) and the subsequent LE emission (400 nm) at the imide moieties in the main chain. The second process is another LE fluorescence consisting of the excitation (340 nm) at the terminal 3HPA moieties followed by the excited-state proton transfer and the subsequent ESIPT emission (530 nm). The third process is a combination of energy transfer and ESIPT processes consisting of the following phenomena: (1) excitation at the imide moieties in the main chain of the PI (340 nm), (2) intra- and/or interchain energy transfer from the imide rings to the 3HPA termini, (3) ESIPT at the 3HPA termini, and (4) ESIPT emission (530 nm). The second and third processes demonstrated a large Stokes' shift (approximately 10000 cm^{-1}) due to the ESIPT occurring at 3HPA.

A Commission Internationale de l'Eclairage (CIE)_1931 chromaticity diagram of the PI-3HPA films with various r values is shown in Figure 14 with their photo images under UV light (365 nm) irradiation. The CIE chromaticity

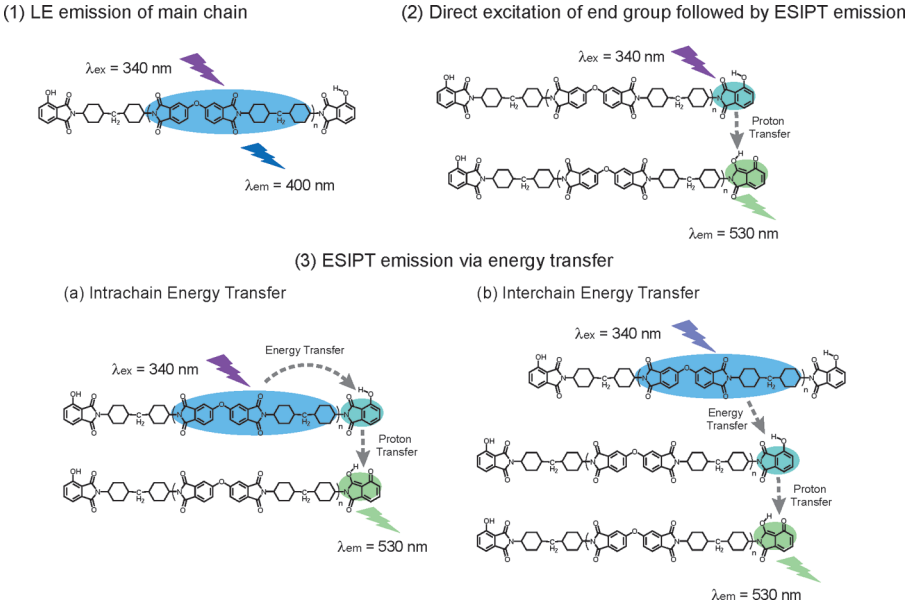

Figure 13. Schematic representation of the excitation and emission mechanism with energy transfer from the imide ring in the main chain (donor) to the 3HPA (acceptor) moiety and ESIPT reaction at the terminus in PI-3HPA films.

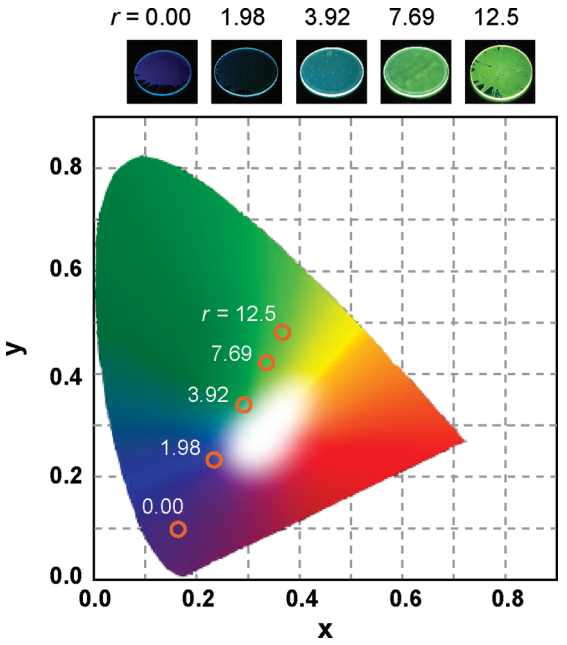

Figure 14. Photo images under UV light (λ = 365 nm) irradiation and emission colors in a CIE chromaticity diagram of PI-ne and PI-3HPA films prepared at various r values: r = 0.00 (0.164, 0.098), r = 1.98 (0.234, 0.233), r = 3.92 (0.292, 0.340), r = 7.69 (0.336, 0.422), and r = 12.5 (0.367, 0.481).

coordinates (x, y) *i.e.* colors of fluorescence, calculated from the emission spectra excited at 365 nm exhibit significant dependence on the ratio of the 3HPA terminus: (x, y) = (0.164, 0.098) for r = 0.00 (blue emission), (0.234, 0.233) for r = 1.98 (light-blue), (0.292, 0.340) for r = 3.92 (white), (0.336, 0.422) for r = 7.69 (light-green), and (0.367, 0.481) for r = 12.5 (light-green). Further, they exhibited significantly high Φ values (9−14%) as solid polymer films with thicknesses of 3.0−15.1 μm (see Tables 4 and 5). As a consequence, the emission color of highly fluorescent PIs can be precisely controlled by varying the molar ratio of the terminus groups which undergo the ESIPT process. In addition, their inherent colorlessness, high optical transparency, and high thermal stability (T_d^5 > 370 °C) are maintained. The molecular design concept for this new type of highly fluorescent PI is beneficial for developing a new class of super engineering plastics for advanced optical and electronic applications.

4. Conclusion

The UV/vis optical absorption and fluorescent properties of imide compounds and PIs having a hydroxy group at the terminal anhydride moiety were extensively examined, and a new molecular design concept for controlling the emission colors of highly fluorescent PIs was established. A weak LE(n−π*) emission at 411 nm (Φ = 0.007) and a strong LE(π−π*) emission at 412 nm (Φ = 0.255) were respectively observed for NHPI and 4HNHPI dissolved in $CHCl_3$. This indicates that the introduction of a hydroxy group into the anhydride moiety of imide compounds significantly lowers the (π−π*) energy level and accordingly enhances the Φ value of LE emission. In addition, 3HNHPI, which can form *intra*-HB, exhibited a strong ESIPT emission at 534 nm with excitation at 332 nm (Φ = 0.352). To the best of our knowledge, this is the first report on an aromatic imide compound exhibiting ESIPT emission with a large Stokes' shift (11394 cm^{-1}). This assignment was verified by the facts that the calculated emission wavelength of the keto−cis tautomer (540 nm) coincides with the observed emission wavelength, and that the LE emission of the enol−cis isomer was observed at 438 nm in a trifluoroacetic acid solution, in which *intra*-HB is disturbed and *inter*-HB is formed with the solvent molecules.

The synthesized PIs, PI-ne, PI-PA, PI-4HPA, and PI-3HPA, showed high transparency in the visible region. Although PI-ne, PI-PA, and PI-4HPA exhibited only LE emission originating from the main chain and/or end groups at around 400 nm, PI-3HPA exhibited two emission peaks at 400 and 530 nm with excitation by UV light. The former and the latter were assignable to LE emission from the main chain and ESIPT emission from the 3HPA termini, respectively. Moreover, the emission intensity at 530 nm relative to that at 400 nm was significantly enhanced by increasing the proportion of fluorescent termini. The fact that the fluorescence lifetime of the LE emission in the imide moieties in the main chain was decreased by increasing the 3HPA termini indicates that the intra- and/or interchain energy transfer should occur from the PI main chain to the termini. As a result, the emission color of PI-3HPA was successfully controlled from blue to light-green through white by varying the amount of terminus groups while maintaining the inherent colorlessness and high transparency. The molecular design concept established in this study should be beneficial for developing a new class of super engineering plastics for advanced optical and electronic applications.

Acknowledgment. We thank Prof. Takashi Yamashita at Tokyo University of Science for his support in fluorescence lifetime measurements and helpful discussions.

Supporting Information Available: Figures showing the calculated IR spectra of the hydrogen-bonded 4HNHPI dimer, the standard and DEPT-135 solution-state ^{13}C NMR spectra of 3HNHPI in $CDCl_3$ and TFA-*d*, the calculated magnetic shielding of 3HNHPI, the ATR FT-IR spectra of PI films, and the TGA curves of PIs, and tables giving the results of TD-DFT calculations of the monocationic species of 3HNHPI and calculated structural parameter of the optimized geometries in the S_0 and S_1 states of 3HNHPI enol−cis and keto−cis forms, a chart showing a model of the monocationic species of 3HNHPI, and a complete ref57. This material is available free of charge via the Internet at http://pubs.acs.org.

References and Notes

(1) Sroog, C. E. *J. Polym. Sci. Macromol. Rev.* **1976**, *11*, 161–208.
(2) Reuter, H.; Franke, H.; Feger, C. *Appl. Opt.* **1988**, *27*, 4565–4571.
(3) Jin, Q.; Yamashita, T.; Horie, K.; Yokota, R.; Mita, I. *J. Polym. Sci., Part A* **1993**, *31*, 2345–2351.
(4) Hasegawa, M.; Shindo, Y.; Sugimura, T.; Ohshima, S.; Horie, K.; Kochi, M.; Yokota, R.; Mita, I. *J. Polymi Sci. B* **1993**, *31*, 1617–1625.
(5) Matsuura, T.; Ando, S.; Sasaki, S.; Yamamoto, F. *Macromolecules* **1994**, *27*, 6665–6670.
(6) Li, Q.; Horie, K.; Yokota, R. *J. Photopolym. Sci. Technol.* **1997**, *10*, 49–54.
(7) Lee, S. A.; Yamashita, T.; Horie, K. *J. Polymi Sci. B* **1998**, *36*, 1433–1442.
(8) Sato, M.; Nakamoto, Y.; Yonetake, K.; Kido, J. *Polym. J.* **2002**, *34*, 601–607.
(9) Hasegawa, M.; Koyanaka, M. *High Perform. Polym.* **2003**, *15*, 47–64.
(10) Hasegawa, M.; Horie, K. *Prog. Polym. Sci.* **2001**, *26*, 259–335.
(11) Li, Q.; Horie, K.; Yokota, R. *Polym. J.* **1998**, *30*, 805–812.
(12) Ishida, H.; Wellinghoff, S. T.; Baer, E.; Koenig, J. L. *Macromolecules* **1980**, *13*, 826–834.
(13) Arjavalingam, G.; Hougham, G.; LaFemina, J. P. *Polymer* **1990**, *31*, 840–844.
(14) Wakita, J.; Sekino, H.; Sakai, K.; Urano, Y.; Ando, S. *J. Phys. Chem. B* **2009**, *113*, 15212–15224.

(15) Matsuda, S.; Urano, Y.; Park, J. W.; Ha, C. S.; Ando, S. *J. Photopolym. Sci. Technol.* **2004**, *17*, 241–246.
(16) Sengupta, P. K.; Kasha, M. *Chem. Phys. Lett.* **1979**, *68*, 382–385.
(17) Ormson, S. M.; Brown, R. G.; Vollmer, F.; Rettig, W. *J. Photochem. Photobiol. A: Chem.* **1994**, *81*, 65–72.
(18) Klymchenko, A. S.; Pivovarenko, V. G.; Demchenko, A. P. *J. Phys. Chem. A* **2003**, *107*, 4211–4216.
(19) Mandal, P. K.; Samanta, A. *J. Phys. Chem. A* **2003**, *107*, 6334–6339.
(20) Holler, M. G.; Campo, L. F.; Brandelli, A.; Stefani, V. *J. Photochem. Photobiol. A: Chem.* **2002**, *149*, 217–225.
(21) Rodembusch, F. S.; Campo, L. F.; Stefani, V.; Rigacci, A. *J. Mater. Chem.* **2005**, *15*, 1537–1541.
(22) Vázquez, S. R.; Rodríguez, M. C. R.; Mosquera, M.; Guez-Prieto, F. R. *J. Phys. Chem. A* **2007**, *111*, 1814–1826.
(23) Ernsting, N. P.; Kovalenko, S. A.; Senyushkina, T.; Saam, J.; Farztdinov, V. *J. Phys. Chem. A* **2001**, *105*, 3443–3453.
(24) Ohshima, A.; Ikegami, M.; Shinohara, Y.; Momotake, A.; Arai, T. *Bull. Chem. Soc. Jpn.* **2007**, *80*, 561–566.
(25) Chu, Q.; Medvetz, D. A.; Pang, Y. *Chem. Mater.* **2007**, *19*, 6421–6429.
(26) Mosquera, M.; Rodríguez, M. C. R.; Rodríguez-Prieto, F. *J. Phys. Chem. A* **1997**, *101*, 2766–2772.
(27) Roberts, E. L.; Dey, J.; Warner, I. M. *J. Phys. Chem. A* **1997**, *101*, 5296–5301.
(28) Fahrni, C. J.; Henary, M. M.; VanDerveer, D. G. *J. Phys. Chem. A* **2002**, *106*, 7655–7663.
(29) Penedo, J. C.; Lustres, J. L. P.; Lema, I. G.; Rodríguez, M. C. R.; Mosquera, M.; Rodríguez-Prieto, F. *J. Phys. Chem. A* **2004**, *108*, 6117–6126.
(30) Tobita, S.; Yamamoto, M.; Kurahayashi, N.; Tsukagoshi, R.; Nakamura, Y.; Shizuka, H. *J. Phys. Chem. A* **1998**, *102*, 5206–5214.
(31) Mishra, H. *J. Phys. Chem. B* **2006**, *110*, 9387–9396.
(32) Catalán, J.; De Paz, J. L. G. *J. Phys. Chem. A* **2008**, *112*, 904–914.
(33) Lewis, J. W.; Sandorfy, C. *Can. J. Chem.* **1982**, *60*, 1727–1737.
(34) Ziółek, M.; Kubicki, J.; Maciejewski, A.; Naskręcki, R.; Grabowska, A. *Phys. Chem. Chem. Phys.* **2004**, *6*, 4682–4689.
(35) Ortiz-Sánchez, J. M.; Gelabert, R.; Moreno, M.; Lluch, J. M. *J. Chem. Phys.* **2008**, *129*, 214308–214318.
(36) Catalán, J.; Del Valle, J. C.; Claramunt, R. M.; Sanz, D.; Dotor, J. *J. Lumin.* **1996**, *68*, 165–170.
(37) Doroshenko, A. O.; Posokhov, E. A.; Verezubova, A. A.; Ptyagina, L. M. *J. Phys. Org. Chem.* **2000**, *13*, 253–265.
(38) Gaenko, A. V.; Devarajan, A.; Tselinskii, I. V.; Ryde, U. *J. Phys. Chem. A* **2006**, *110*, 7935–7942.
(39) Chou, P. T.; McMorrow, T. J. A.; Kasha, M. *J. Phys. Chem.* **1984**, *88*, 4596–4599.
(40) Chou, P. T.; Martinez, M. L. *Radiat. Phys. Chem.* **1993**, *41*, 373–378.
(41) Stein, M.; Keck, J.; Waiblinger, F.; Fluegge, A. P.; Kramer, H. E. A.; Hartschuh, A.; Port, H.; Leppard, D.; Rytz, G. *J. Phys. Chem. A* **2002**, *106*, 2055–2066.
(42) Sytnik, A.; Del Valle, J. C. *J. Phys. Chem.* **1995**, *99*, 13028–13032.
(43) Kang, J. W.; Kim, S.; Park, S. Y.; Kim, J. J. *Appl. Phys. Lett.* **2004**, *84*, 4221–4223.
(44) Park, S.; Kwon, J. E.; Kim, S. H.; Seo, J.; Chung, K.; Park, S. Y.; Jang, D. J.; Medina, B. M.; Gierschner, J.; Park, S. Y. *J. Am. Chem. Soc.* **2009**, *131*, 14043–14049.
(45) Ogoshi, T.; Miyake, J.; Chuji, Y. *Macromolecules* **2005**, *38*, 4425–4431.
(46) Park, S.; Kim, S.; Seo, J.; Park, S. Y. *Macromolecules* **2005**, *38*, 4557–4559.
(47) Kim, S.; Seo, J.; Jung, H. K.; Kim, J. J.; Park, S. Y. *Adv. Mater.* **2005**, *17*, 2077–2082.
(48) Lee, J. K.; Kim, H. J.; Kim, T. H.; Lee, C. H.; Park, W. H.; Kim, J.; Lee, T. S. *Macromolecules* **2005**, *38*, 9427–9433.
(49) Kim, T. H.; Kim, H. J.; Kwak, C. G.; Park, W. H.; Lee, T. S. *J. Polym. Sci., Part A* **2006**, *44*, 2059–2068.
(50) Campo, L. F.; Rodembusch, F. S.; Stefani, V. *J. Appl. Polym. Sci.* **2006**, *99*, 2109–2116.
(51) Matsumoto, T. *High Perform. Polym.* **1999**, *11*, 367–377.
(52) Oishi, Y.; Ogasawara, K.; Hirahara, H.; Mori, K. *J. Photopolym. Sci. Technol.* **2001**, *14*, 37–40.
(53) Oishi, Y.; Kikuchi, N.; Mori, K.; Ando, S.; Maeda, K. *J. Photopolym. Sci. Technol.* **2002**, *15*, 213–214.
(54) Lee, C.; Yang, W.; Parr, R. G. *Phys. Rev.* **1988**, *B37*, 785–789.
(55) Miehlich, B.; Savin, A.; Stoll, H.; Preuss, H. *Chem. Phys. Lett.* **1989**, *157*, 200–206.
(56) Becke, A. D. *J. Chem. Phys.* **1993**, *98*, 5648–5652.
(57) Frisch, M. J.; et al. *Gaussian 09, Revision A.02*; Gaussian, Inc.: Wallingford CT, 2009.
(58) Steiner, T. *Angew. Chem., Int. Ed.* **2002**, *41*, 48–76.
(59) Chen, Y.; Topp, M. R. *Chem. Phys.* **2002**, *283*, 249–268.
(60) Bilton, C.; Allen, F. H.; Shields, G. P.; Howard, J. A. K. *Acta Crystallogr.* **2000**, *B56*, 849–856.
(61) Turro, N. J. In *Modern Molecular Photochemistry*; University Science Books: Sausalito, CA, 1999; p 87, 177.
(62) Coyle, J. D.; Newport, G. L. *Tetrahedron Lett.* **1977**, *18*, 899–902.
(63) Coyle, J. D.; Harriman, A.; Newport, G. L. *J. Chem. Phys., Perkin Trans. II* **1979**, 799–802.
(64) Yamanzaki, I.; Tami, N.; Yamazaki, T. *J. Phys. Chem.* **1990**, *94*, 516–525.